CHAPTER 5

Geostatistical Inversion Results

Geostatistical inversion were produced using the RockMod module in Jason software, and covered an area of 85 km^2 (see Figure 5.1). The geostatistical inversion process is very computationally intensive and required several days to finish. Based on the tested parameters which is discussed in Chapter 4, multi-realizations of lithofacies and elastic property cubes were produced based on the best inversion parameter set (Test 18). In order to QC inversion results, several visual aids were included. Such as arbitrary section of all inversion products overlaid with well log data, stratigraphic slices of lithology and probability volumes, comparisons with deterministic inversion results, and “blind” validation well QC.

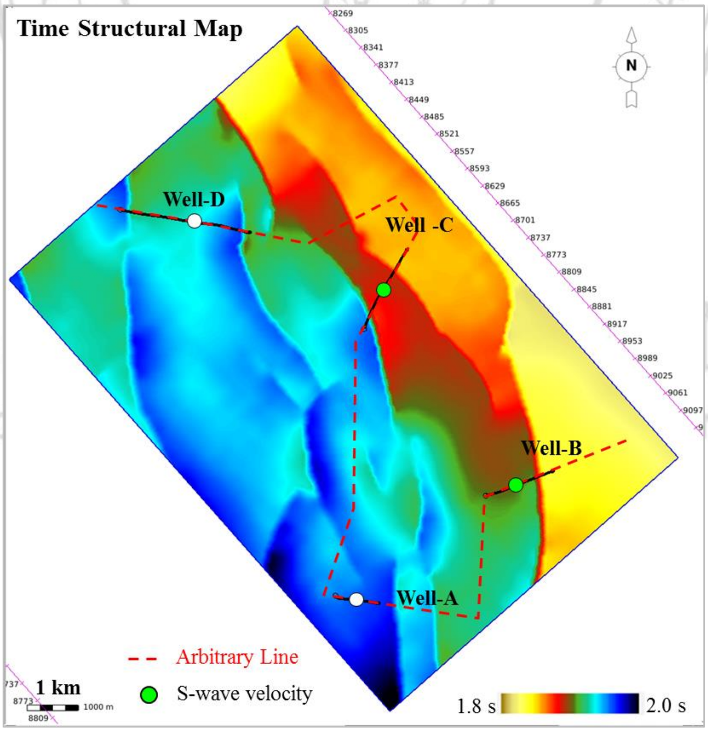

Figure 5.1 Geostatistical inversion area covering 85 km^2 and arbitrary line passing through four input wells.

5.1 Geostatistical Inversion Results

Based on the final inversion parameter set (Test 18), ten realizations of geostatistical inversions were generated in order to capture a reasonable range of possible inversion results, including lithofacies and elastic property volumes (P-Impedance, Vp/Vs and density). Inversion results from three of these realizations, consisting of realization 3, 6 and 9 were selected to demonstrate the variety of lithology and elastic property distributions, and compared to input well data as shown in Figure 5.2 to 5.4 (remaining realizations shown in Appendix B).

Results obtained from realizations 3, 6 and 9 showed that lithofacies and AI sections were conforming to well data and provided reasonable sand thickness and distribution in these realizations. In general, the thicker sand bodies were represented in a similar manner for all three realizations and probably driven by the seismic amplitude trends; whereas, thin sands were random in each realization following geostatistics derived from well logs and seismic data. However, Vp/Vs and density sections showed moderate to poor correlation with well data. Inverted Vp/Vs and density provided the correct overall trend, but could not capture details. This was possibly caused by short streamer offset which provided insufficient far angle data and relatively poor seismic data quality to conduct density and Vp/Vs estimation.

To validate and QC all realizations in an effective manner, statistical volumes including mean, standard deviation and probability volumes were generated using the complete inversion results from all ten realizations. Figure 5.5 shows most probable lithofacies and mean inverted elastic property cubes calculated from all ten realizations. Overall, the mean case of all realizations highlighted only the thicker sand bodies. Thinner sands and coals were distributed in a more random pattern and were therefore averaged out. This is a common observation for geostatistical inversion, as such mean elastic property volumes tend to share similarities with deterministic inversion results.

As part of the QC, the seismic residuals (original seismic – synthetic) after inversion compared to the original seismic was also considered. Input parameters should be selected to produce low residual magnitude with a random pattern, and thereby representing noise instead of geological features. Figures 5.6 to 5.9 show initial angle stacks, synthetic (calculated from inverted elastic properties) and residual of near, near-mid, mid and far seismic stacks (from realization 6). From these results it can be seen that these residuals showed slightly higher magnitude for near angle seismic data, and probably caused by noise, while such residuals were of lower magnitude for near-mid and mid angle seismic data. The residual magnitudes were increasing for the far angle seismic data, and probably caused by reduced seismic data quality, often observed in far offset data.

In addition, horizon slices of both reservoir layers (H30 and H37) were generated to observed lateral distribution of each lithology type and inverted elastic properties. Horizon slice from reservoir 1 (H30) show in Figure 5.10 to 5.12. In general, positive seismic amplitude provided low AI, low Vp/Vs and low density which showed high probability of sand. As shown in Figure 5.10, channel like feature was observed in sand probability map (N-S direction) that consistent with positive amplitude, low AI, low Vp/Vs and low density. In reservoir 2 (H37), the strongest positive amplitude in seismic were related to coal which showed lowest AI, lowest density and moderate Vp/Vs (see Figure 5.13). In Figure 5.14, it is difficult to observe the geological features in horizon slice of AI slice due to low AI contrast between sand and shale. However, sand bodies (high probability of sand) in this horizon slice could be classified with moderate to low Vp/Vs and density.

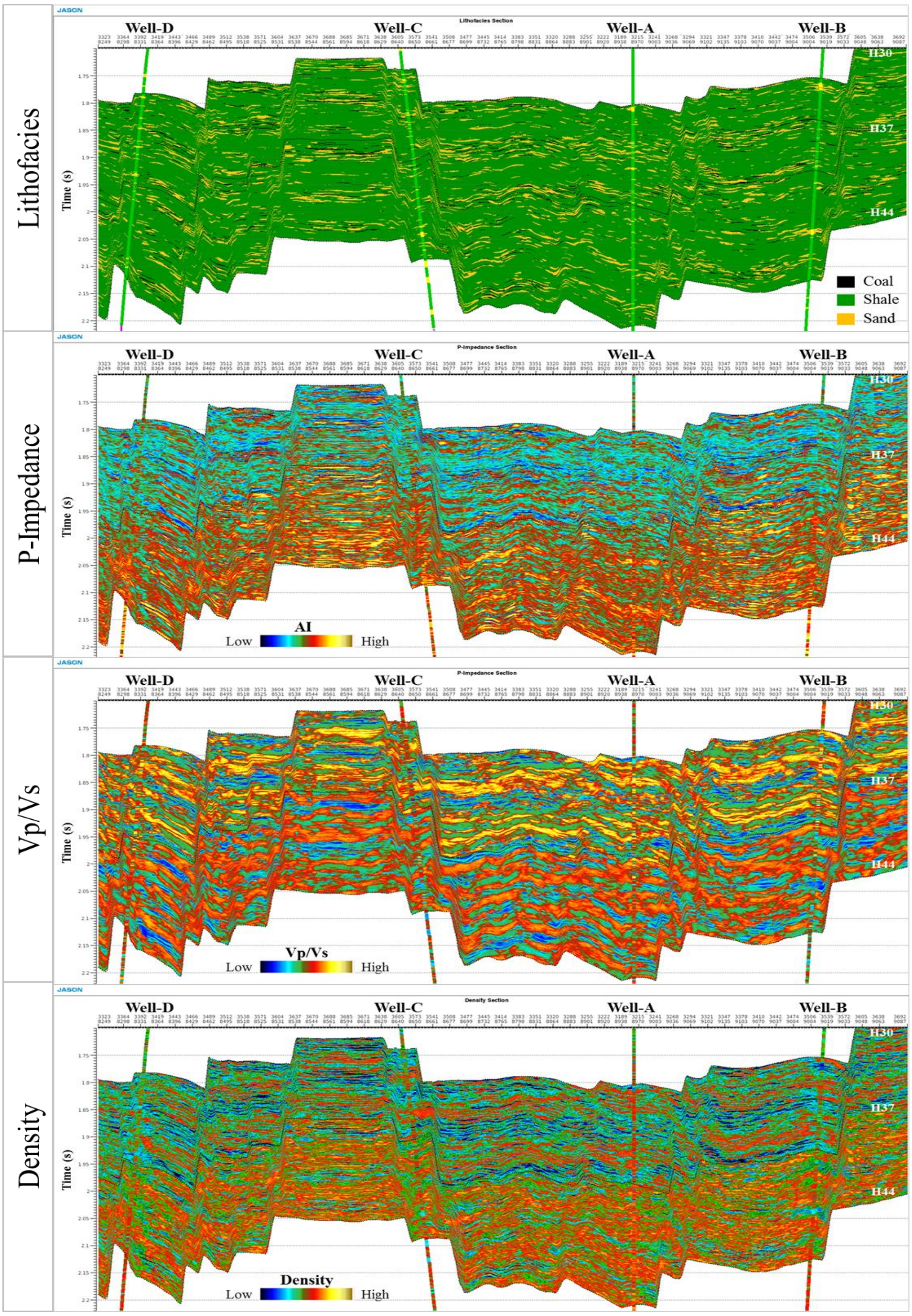

Figure 5.2 Geostatistical inversion results, including lithofacies, P-Impedance, Vp/Vs and density generated from inversion realization 3, with respective well log data superposed.

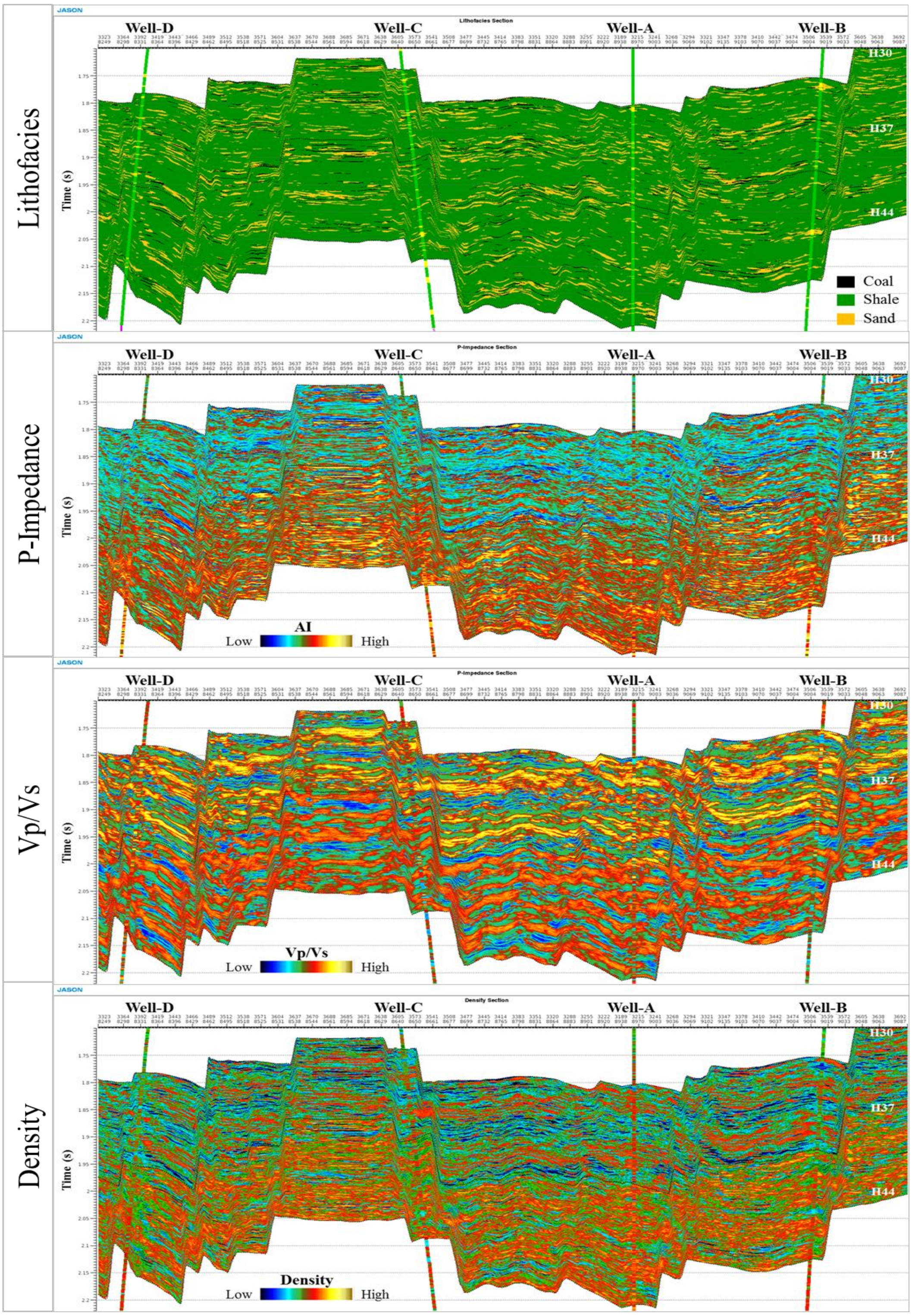

Figure 5.3 Geostatistical inversion results, including lithofacies, P-Impedance, Vp/Vs and density generated from inversion realization 6, with respective we ll log data superposed.

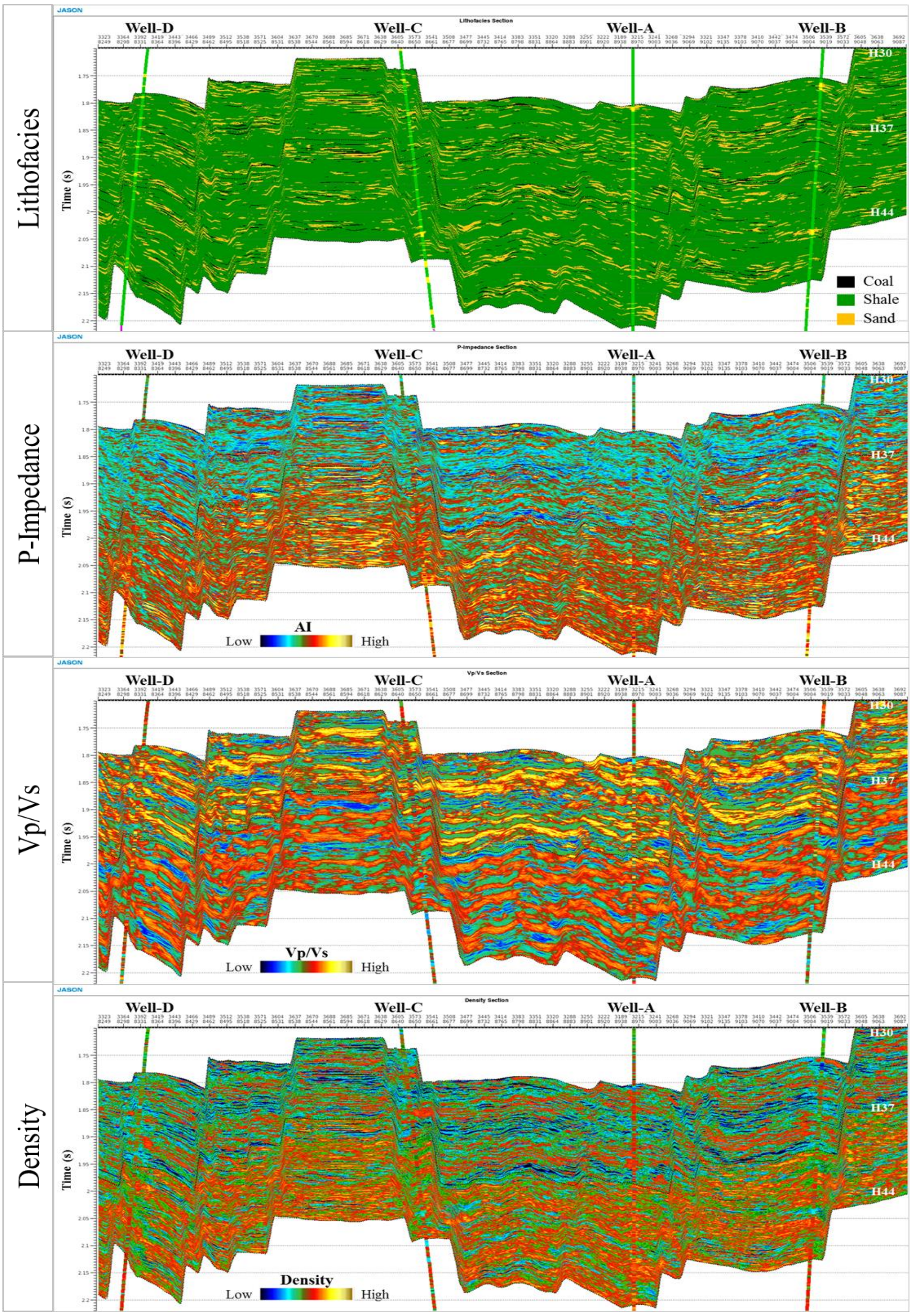

Figure 5.4 Geostatistical inversion results, including lithofacies, P-Impedance, Vp/Vs and density generated from inversion realization 9, with respective well log data superposed.

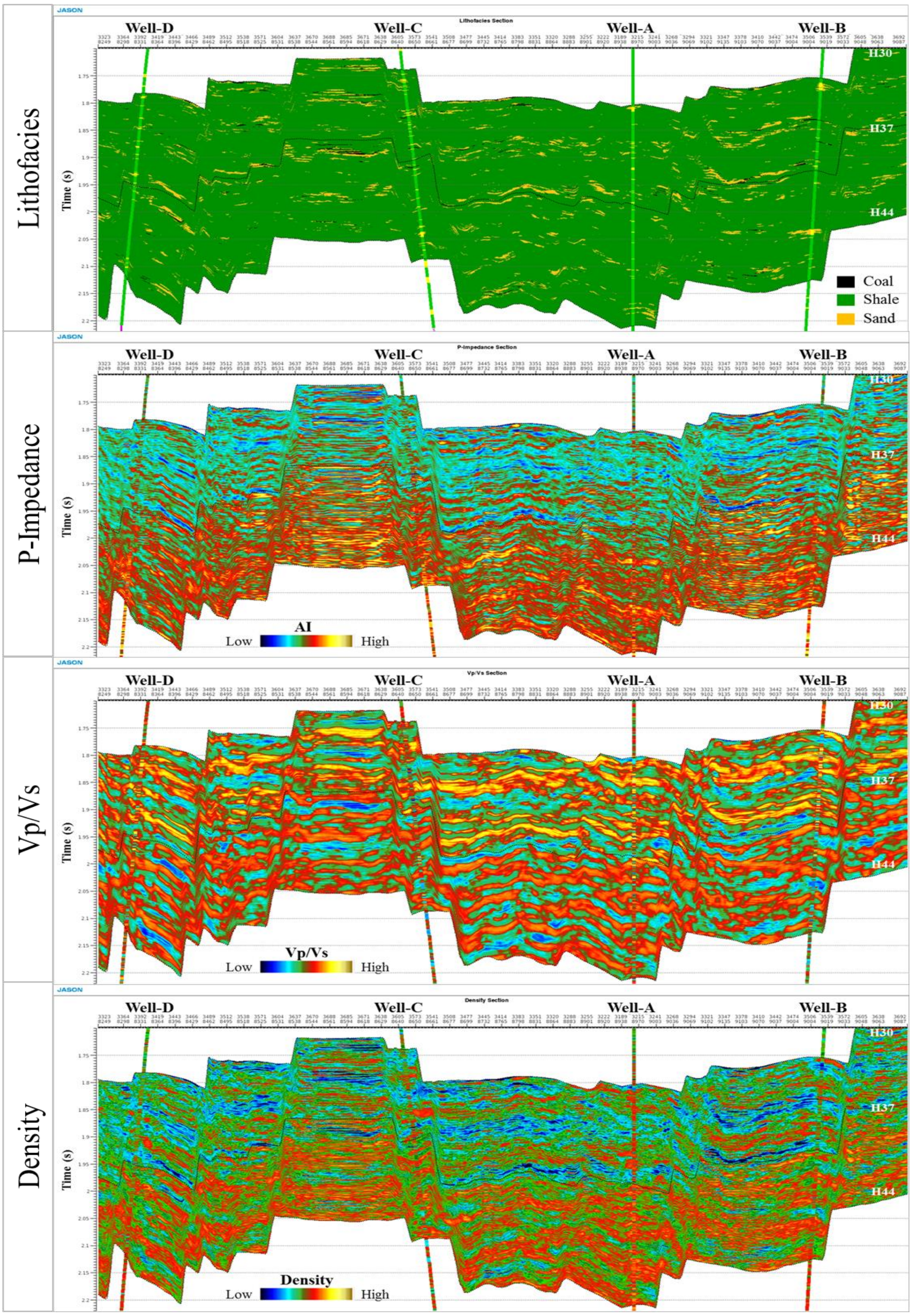

Figure 5.5 Geostatistical inversion results, including lithofacies, P-Impedance, Vp/Vs and density generated from mean of ten realizations, with respective well log data superposed.

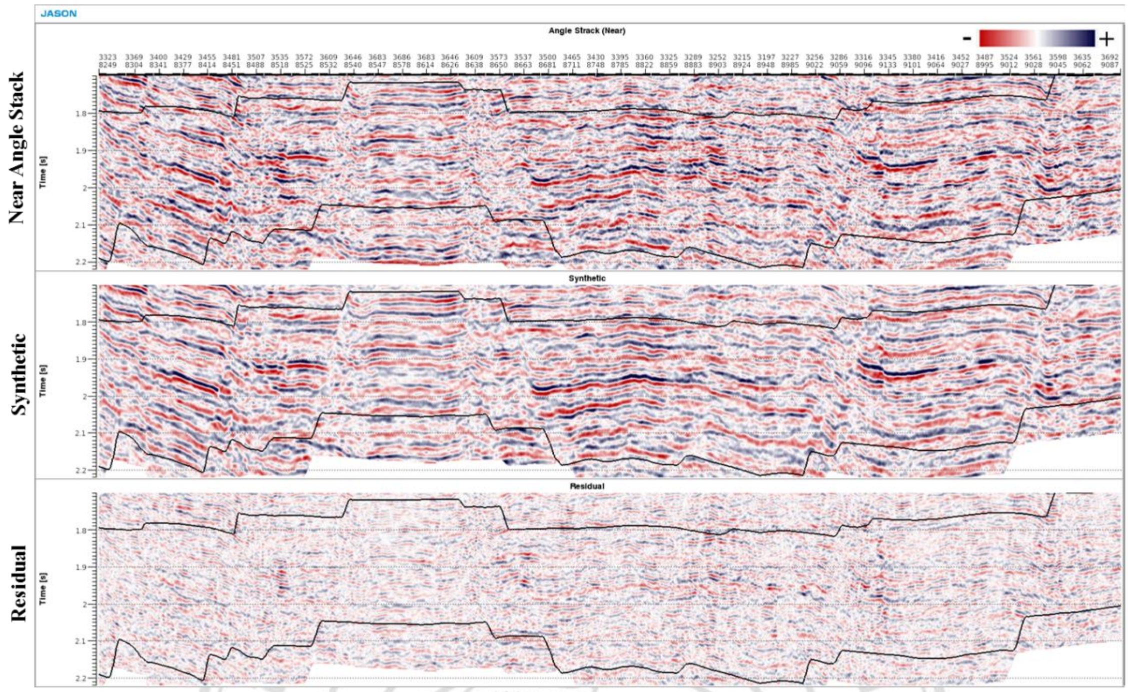

Figure 5.6 Comparison of seismic near angle stack, synthetic and remaining residuals generated from realization 6.

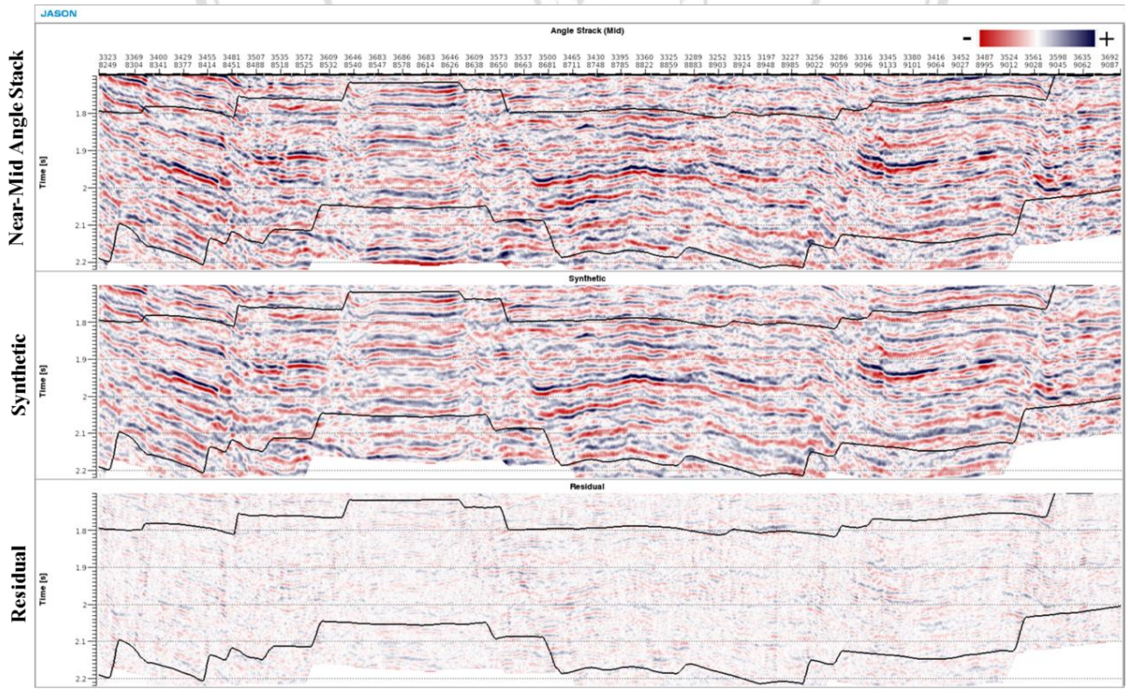

Figure 5.7 Comparison of seismic near-mid angle stack, synthetic and remaining residuals generated from realization 6.

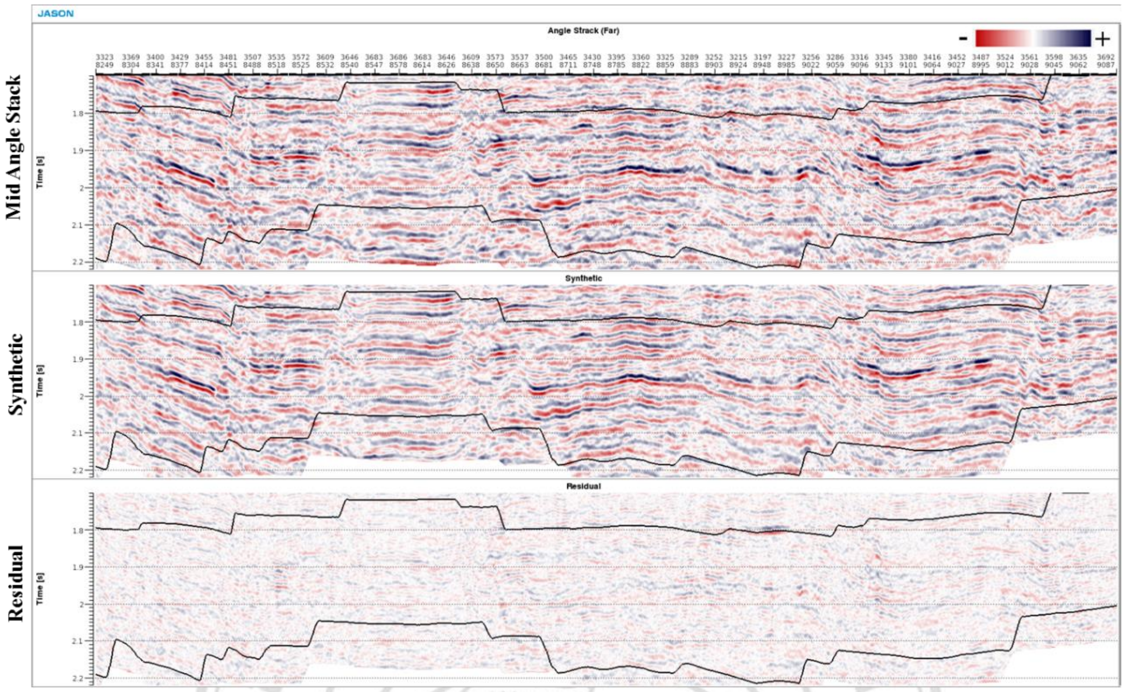

Figure 5.8 Comparison of seismic mid angle stack, synthetic and remaining residuals generated from realization 6.

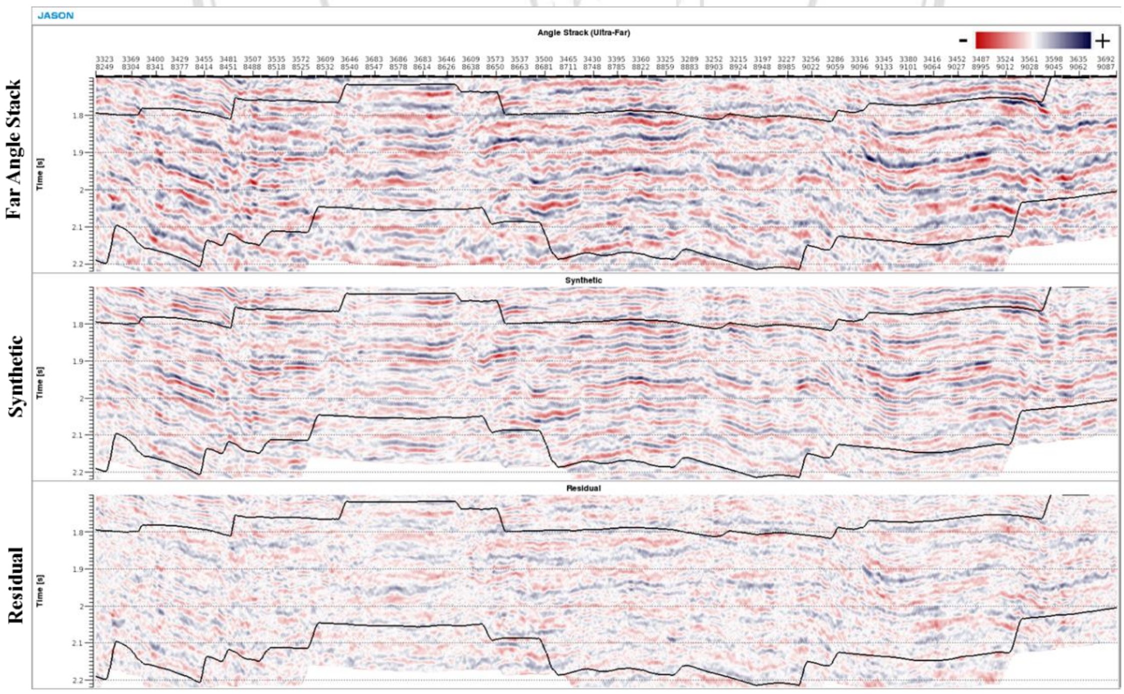

Figure 5.9 Comparison of seismic far angle stack, synthetic and remaining residuals generated from realization 6.

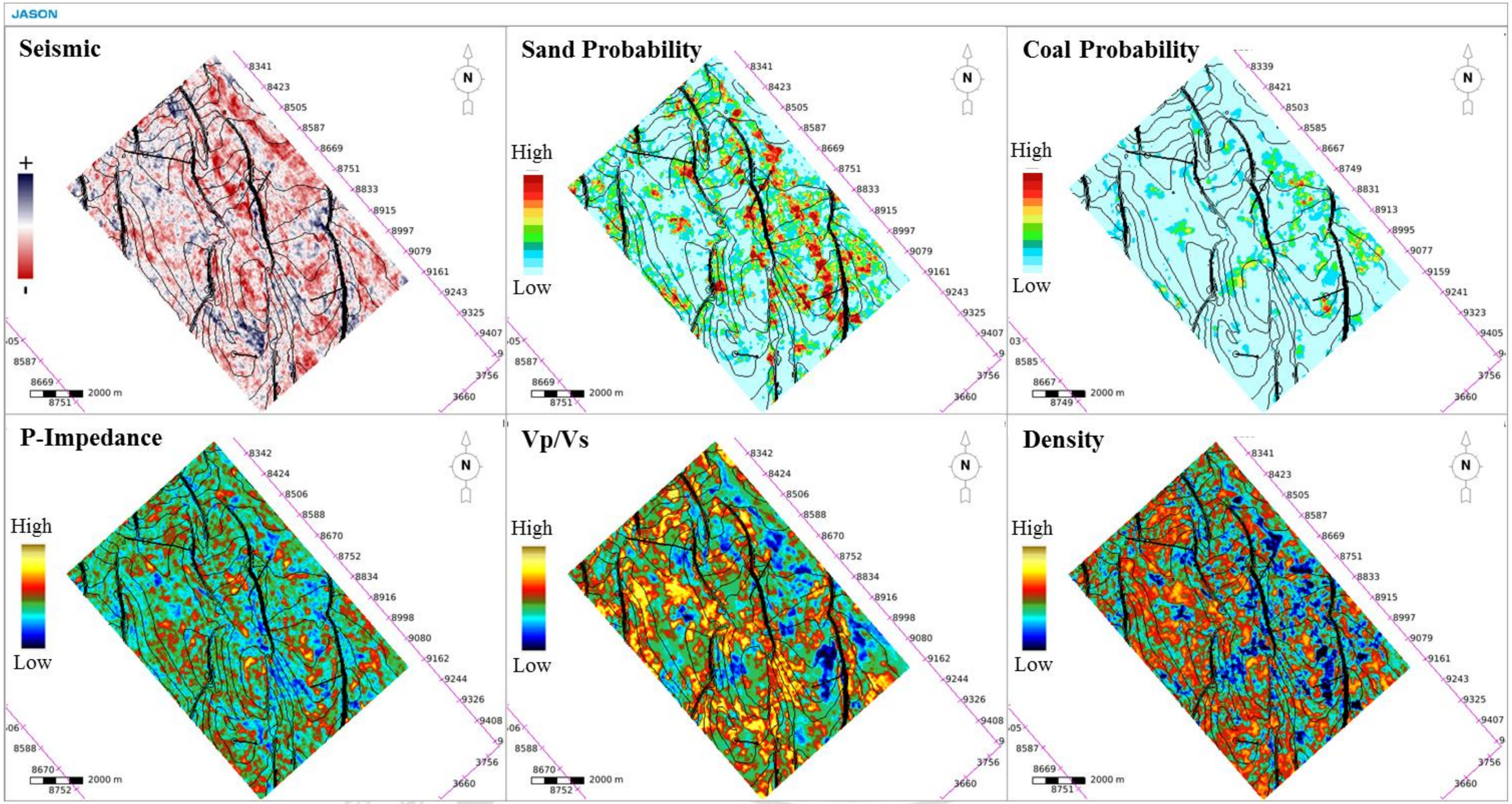

Figure 5.10 Horizon slices of seismic, probability and elastic properties (AI, Vp/Vs and density) along reservoir 1-1 (H30)

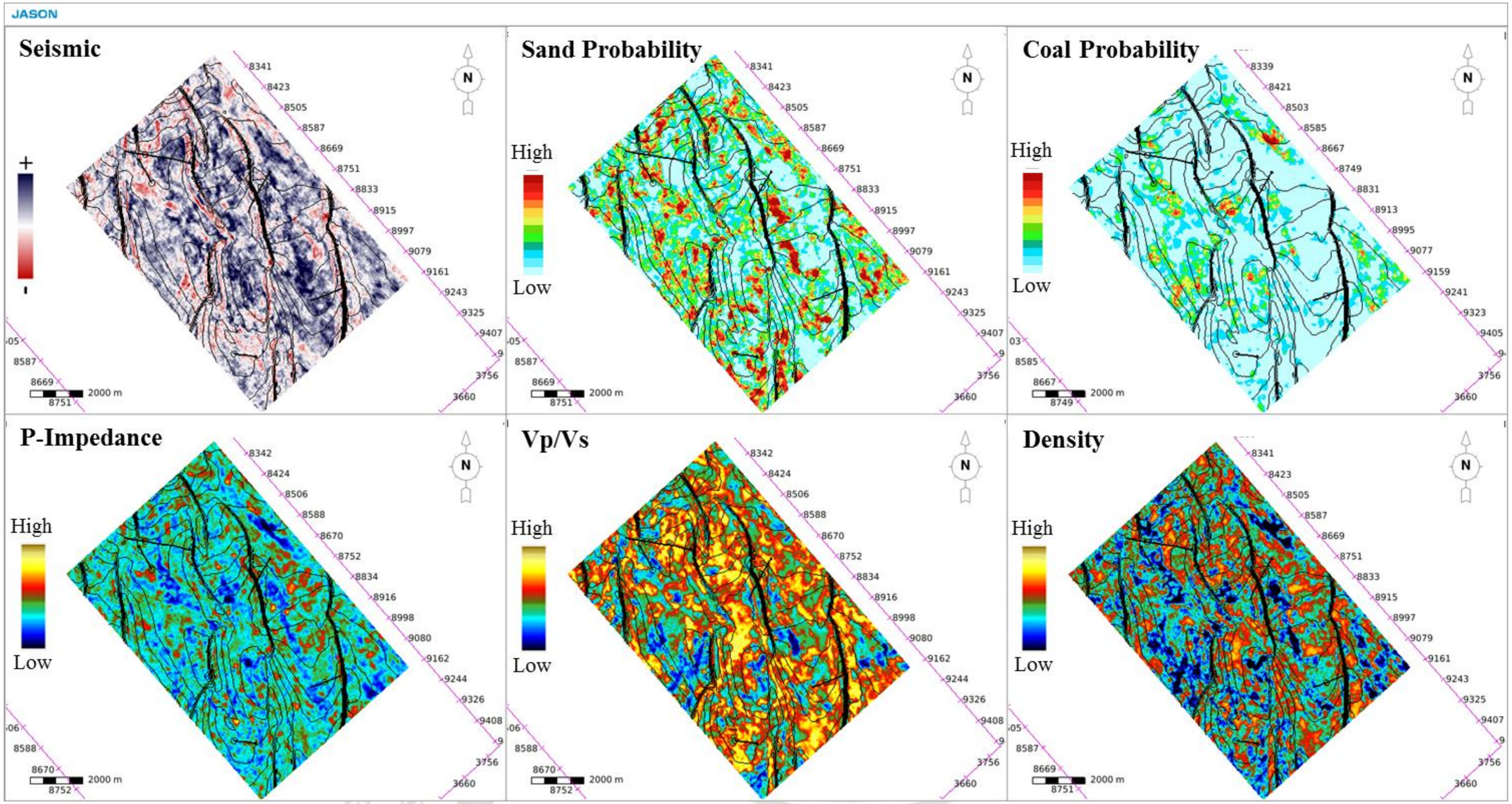

Figure 5.11 Horizon slices of seismic, probability and elastic properties (AI, Vp/Vs and density) along reservoir 1-2 (H30)

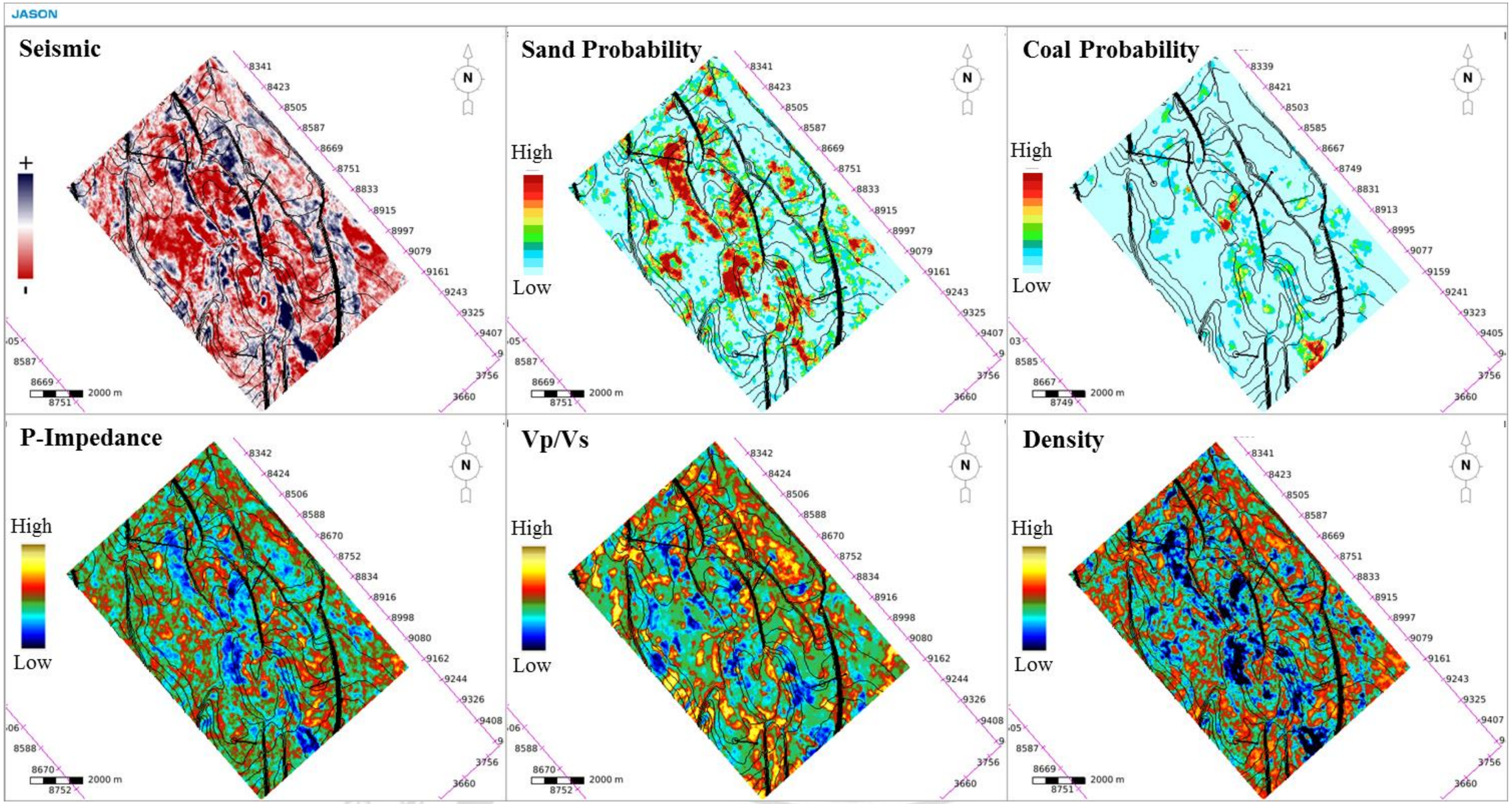

Figure 5.12 Horizon slices of seismic, probability and elastic properties (AI, Vp/Vs and density) along reservoir 1-3 (H30)

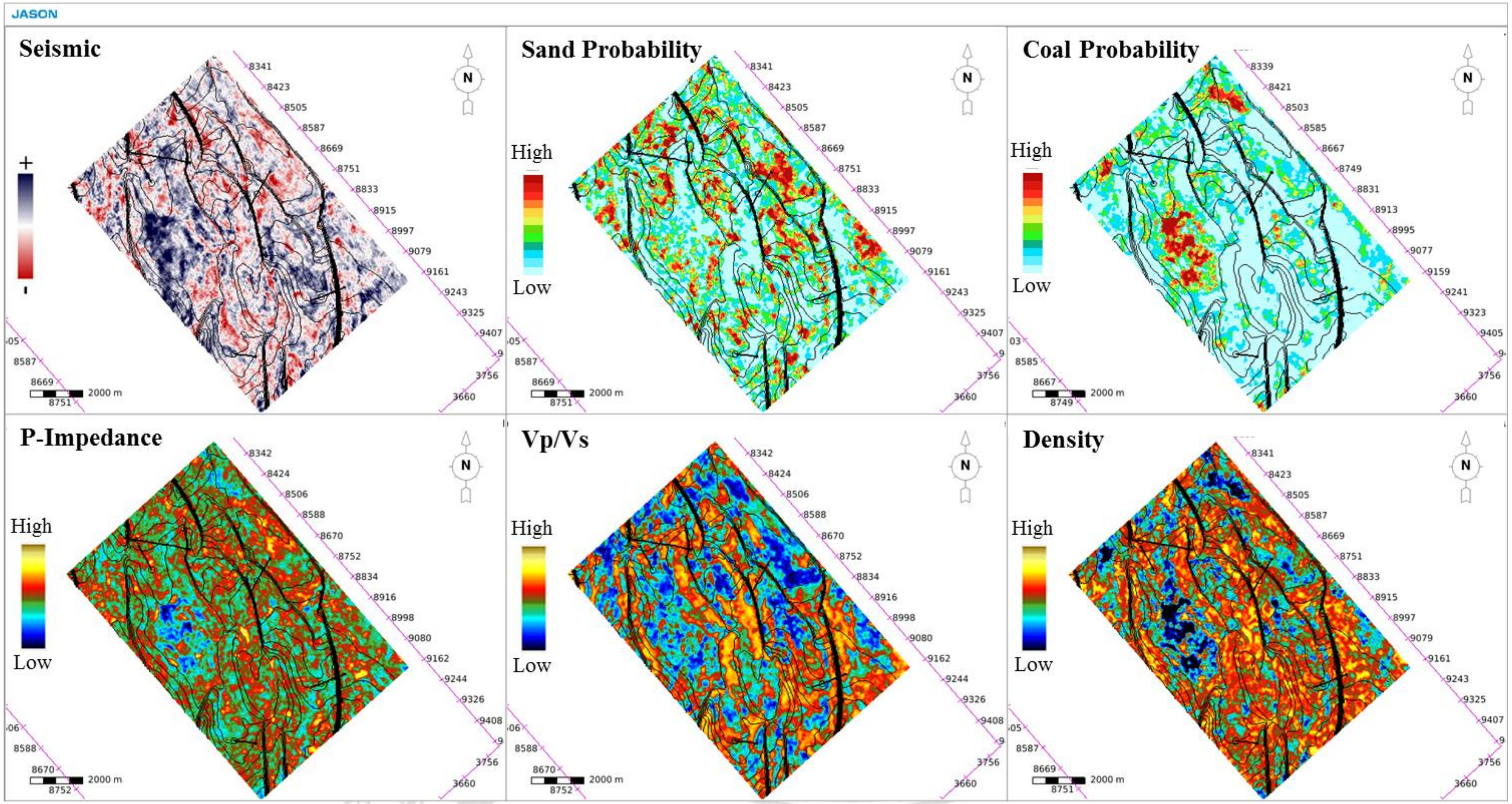

Figure 5.13 Horizon slices of seismic, probability and elastic properties (AI, Vp/Vs and density) along reservoir 2-1 (H37)

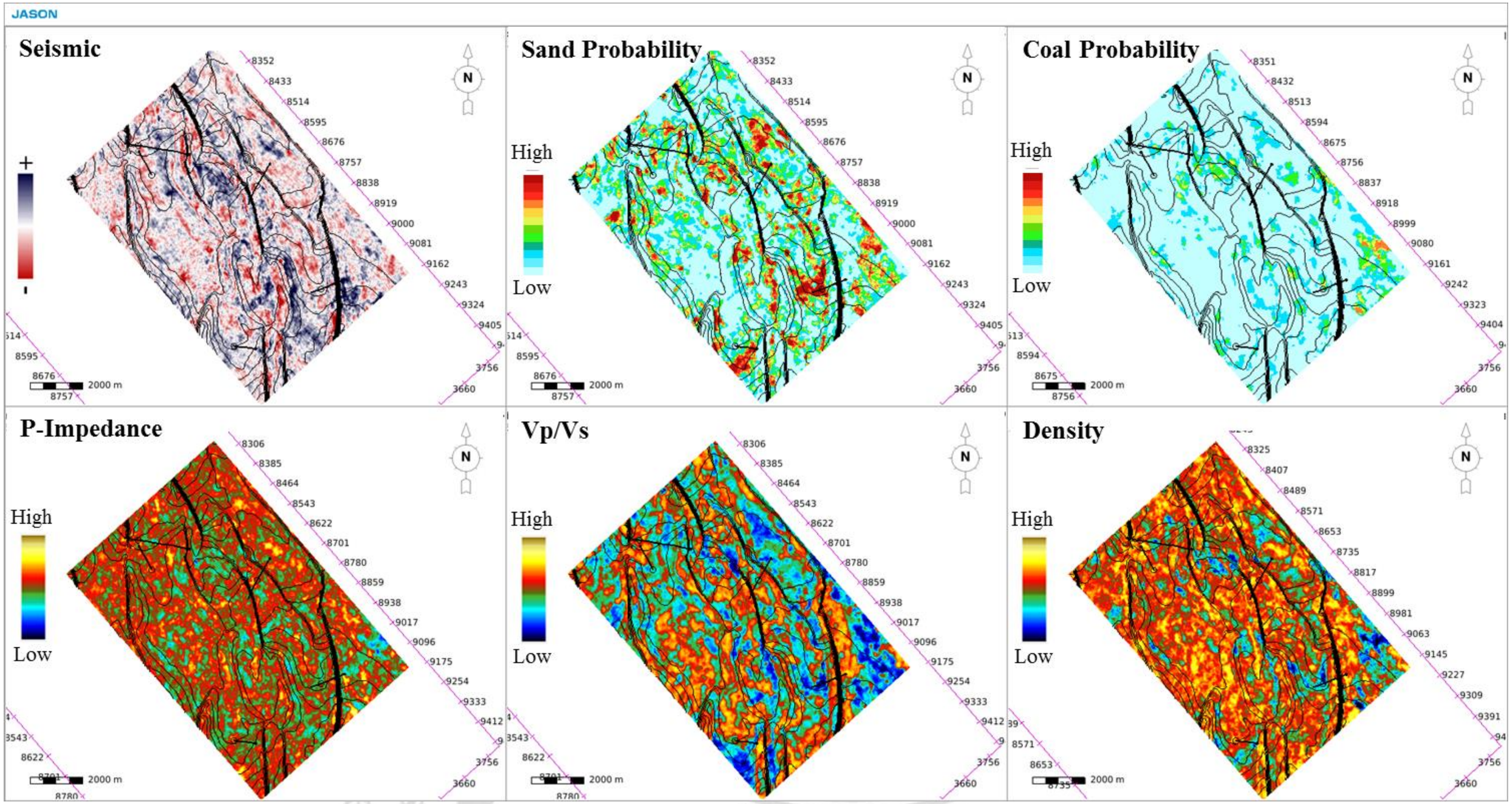

Figure 5.14 Horizon slices of seismic, probability and elastic properties (AI, Vp/Vs and density) along reservoir 2-2 (H37)

5.2 Comparison of Deterministic and Geostatistical Inversion

To verify the quality of the geostatistical inversion results, most probable lithofacies and mean elastic properties, such as AI and Vp/Vs, were generated and compared to the deterministic inversion results as demonstrated in Figure 5.15 to 5.17. In lithofacies section (Figure 5.15), both deterministic and geostatistical inversions tend to predict sand at similar location, but the geostatistical inversion method provided better resolution that can identify geological detail at a much smaller scale such as thin sands and coals. In some locations, the results of deterministic inversion method shows overestimated sand thicknesses, which might be the result of seismic tuning effects. This might lead to overestimation of sand in some locations, while in other locations the deterministic cannot account for any sands, as they are below seismic detectability and therefore not observed in the deterministic inversion results.

As can be seen in Figure 5.16, both geostatistical and deterministic inversions show a similar depth trend for AI, which is increasing with depth. However, the resulting AI derived from geostatistical inversion provided improved resolution that were conforming to well log data. Regarding thicker sand bodies, both deterministic and geostatistical inversion results show similar AI trends and values. Comparisons of the resulting Vp/Vs sections following deterministic and geostatistical inversions (see Figure 5.17), clearly indicate that these methods provide different results. The overall trends are different, but most striking is the higher resolution and improved correlation to wells provided by the geostatistical inversion results.

Besides section views, horizon slices of sand probability and lithofacies volumes were generated to QC the results derived from geostatistical inversion. The comparison of horizon slices extracted from Reservoir H30 layer 1-1 from deterministic and geostatistical inversion can be seen in Figures 5.18 to 5.21. As shown in Figure 5.18, channel like features were observed at Well-B by both deterministic and geostatistical inversion results at this level. However, due to the overestimation of sand thickness from the deterministic inversion results, and contrary to well log data, the same channel feature was also observed in the layer below (H30 layer 1-2) for both sand probability and lithofacies, while it was not observed in the geostatistical inversion results at this level (see Figure 5.19). Sand probability and lithofacies slices from Reservoir H37 layer 2-1 can be seen in Figures 5.20 and 5.21. Sand probability maps resulting from the geostatistical inversion indicates smaller sand bodies than results obtained from deterministic inversion, which often overestimates the size of sand bodies both vertically and laterally.

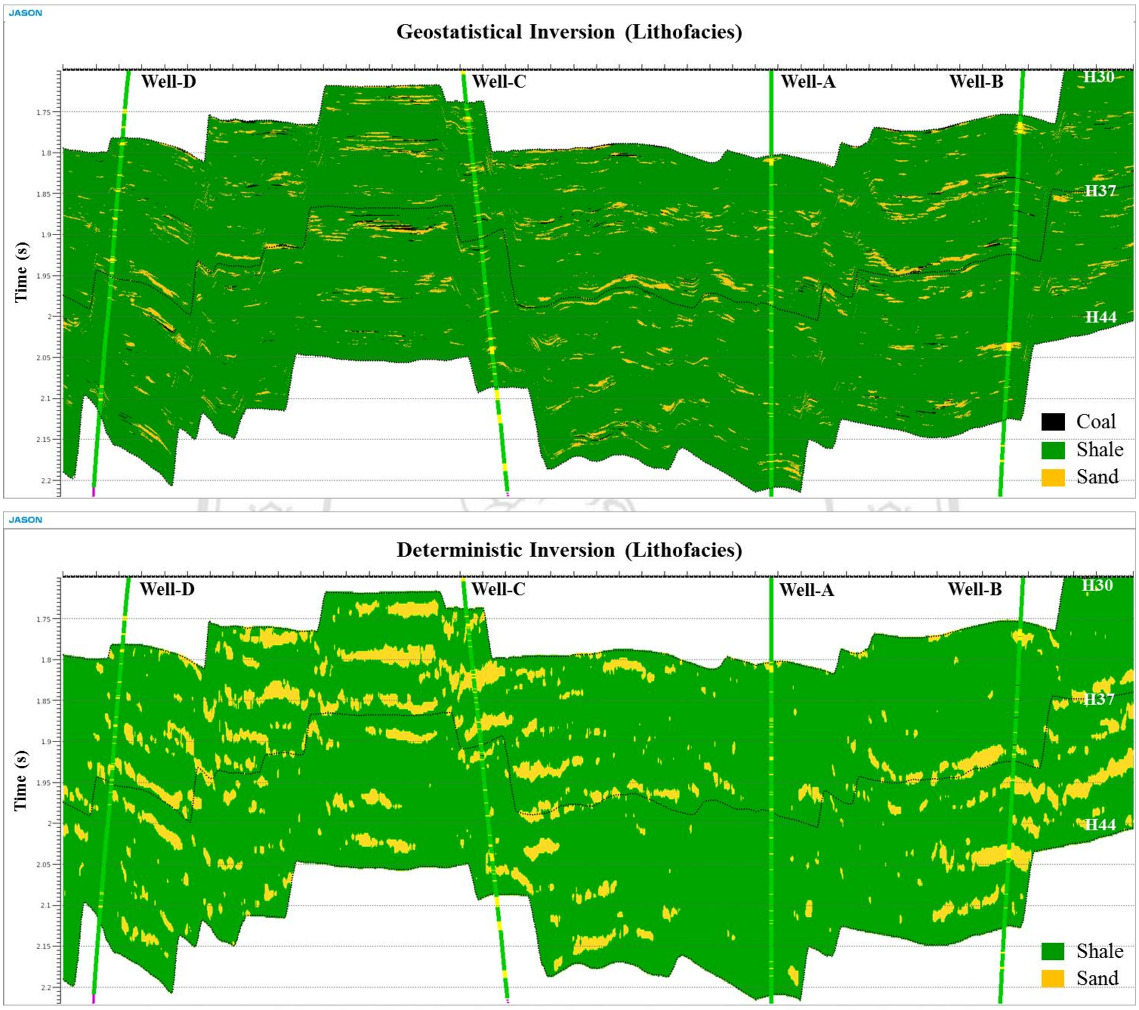

Figure 5.15 Comparison of lithofacies sections from geostatistical inversion (above) and deterministic inversion (below).

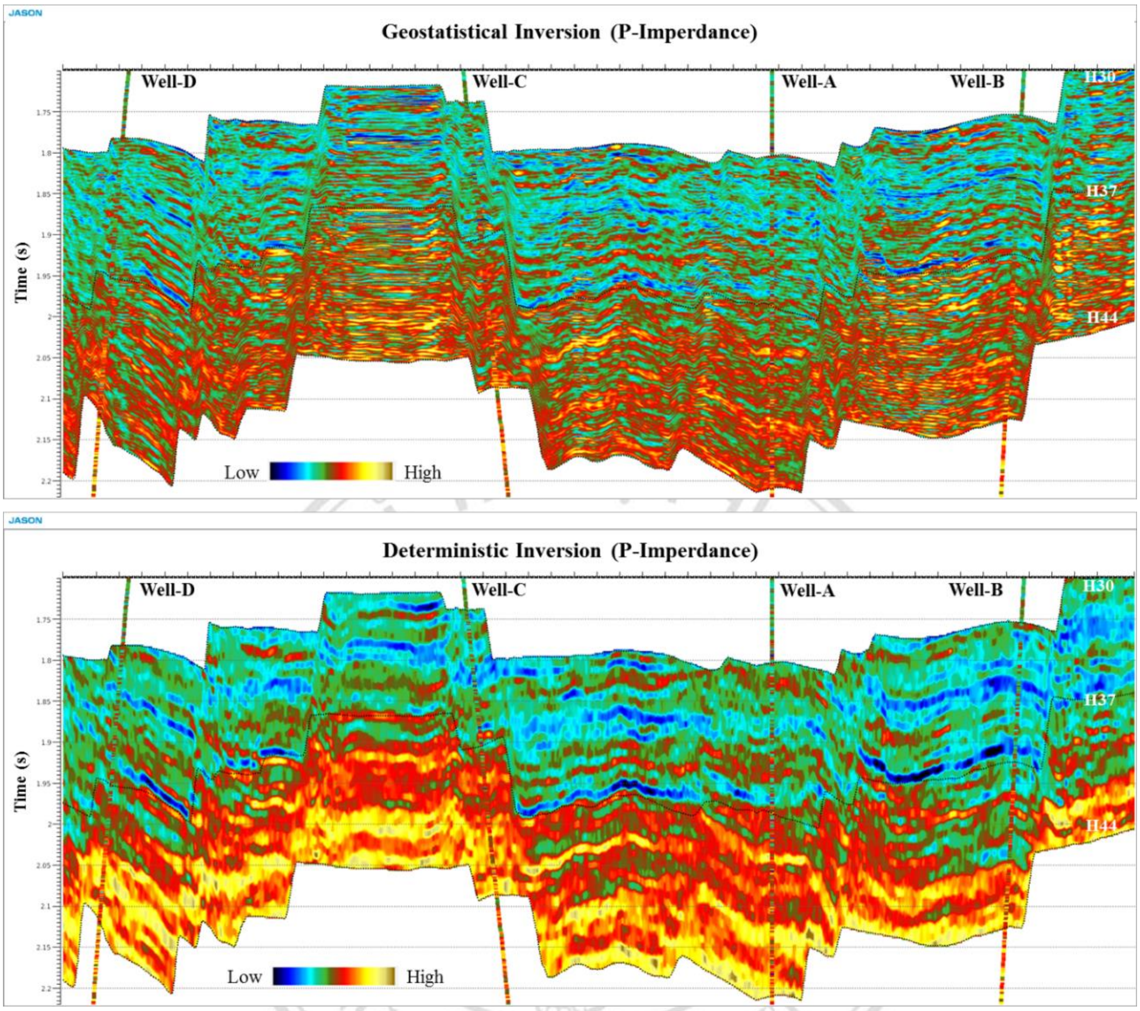

Figure 5.16 Comparison of P-Impedance sections from geostatistical inversion (above) and deterministic inversion (below).

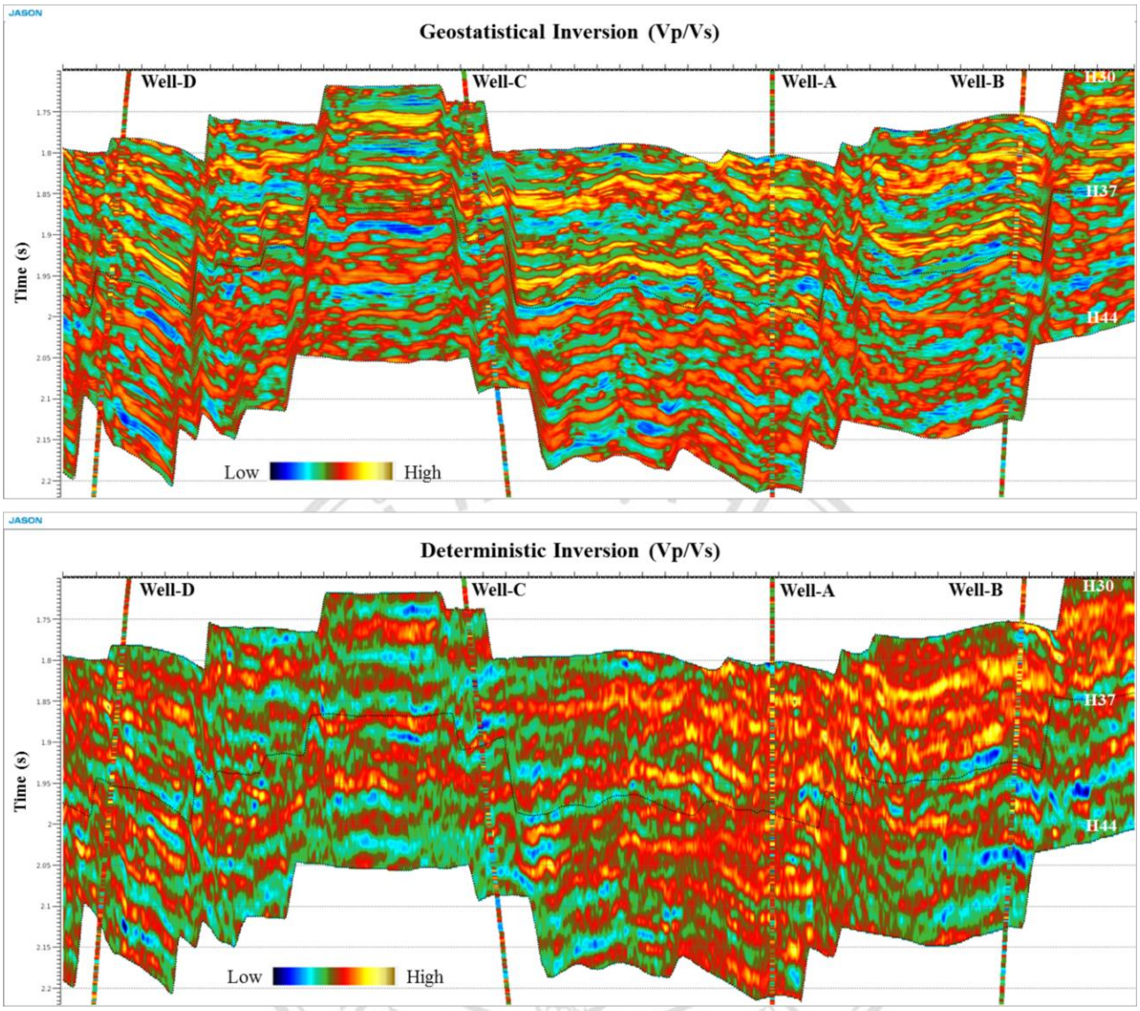

Figure 5.17 Comparison of Vp/Vs sections from geostatistical inversion (above) and deterministic inversion (below).

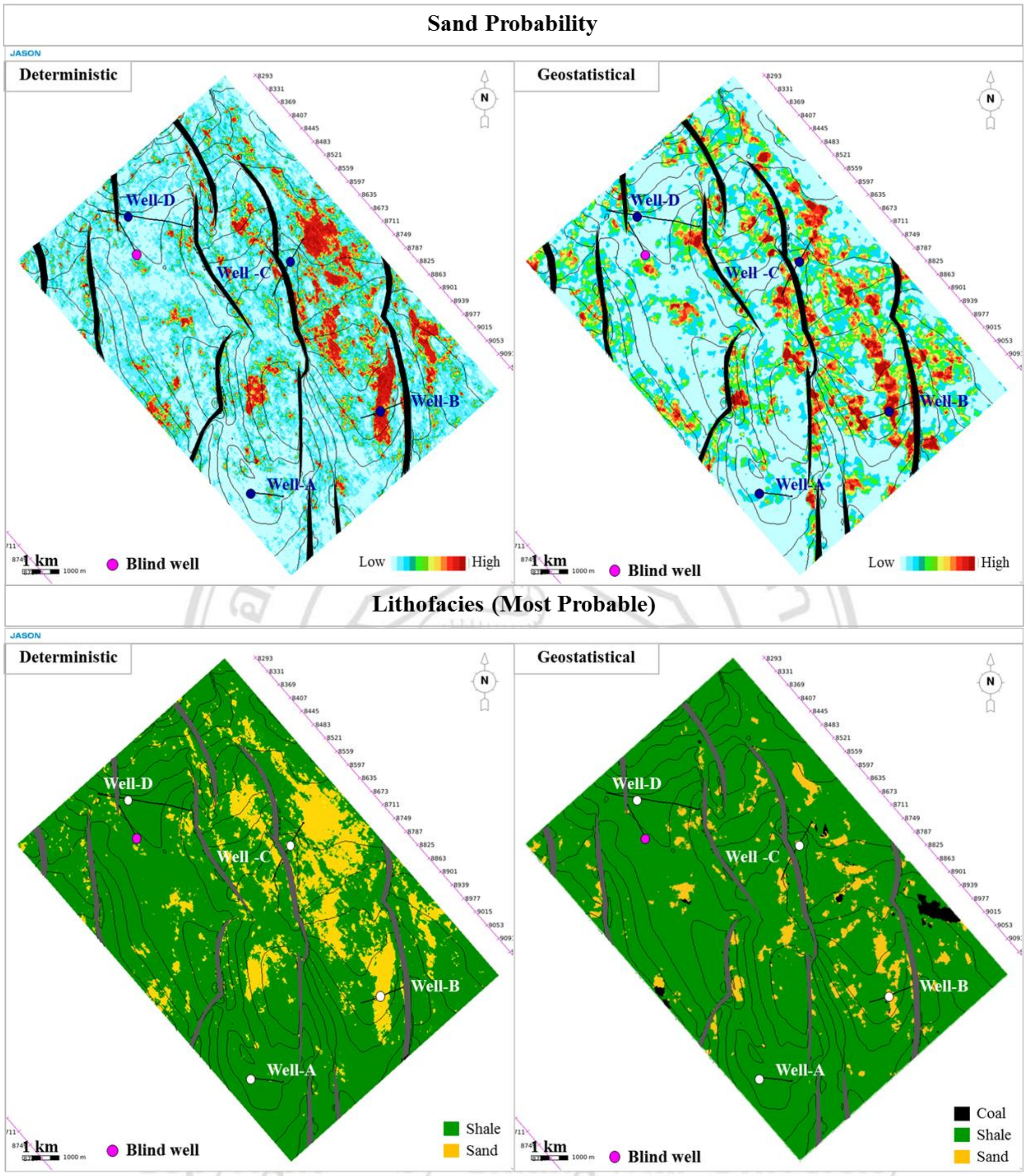

Figure 5.18 Sand probability and lithofacies slices at Reservoir 1-1 layer (H30) from deterministic (left) and geostatistical inversion (right).

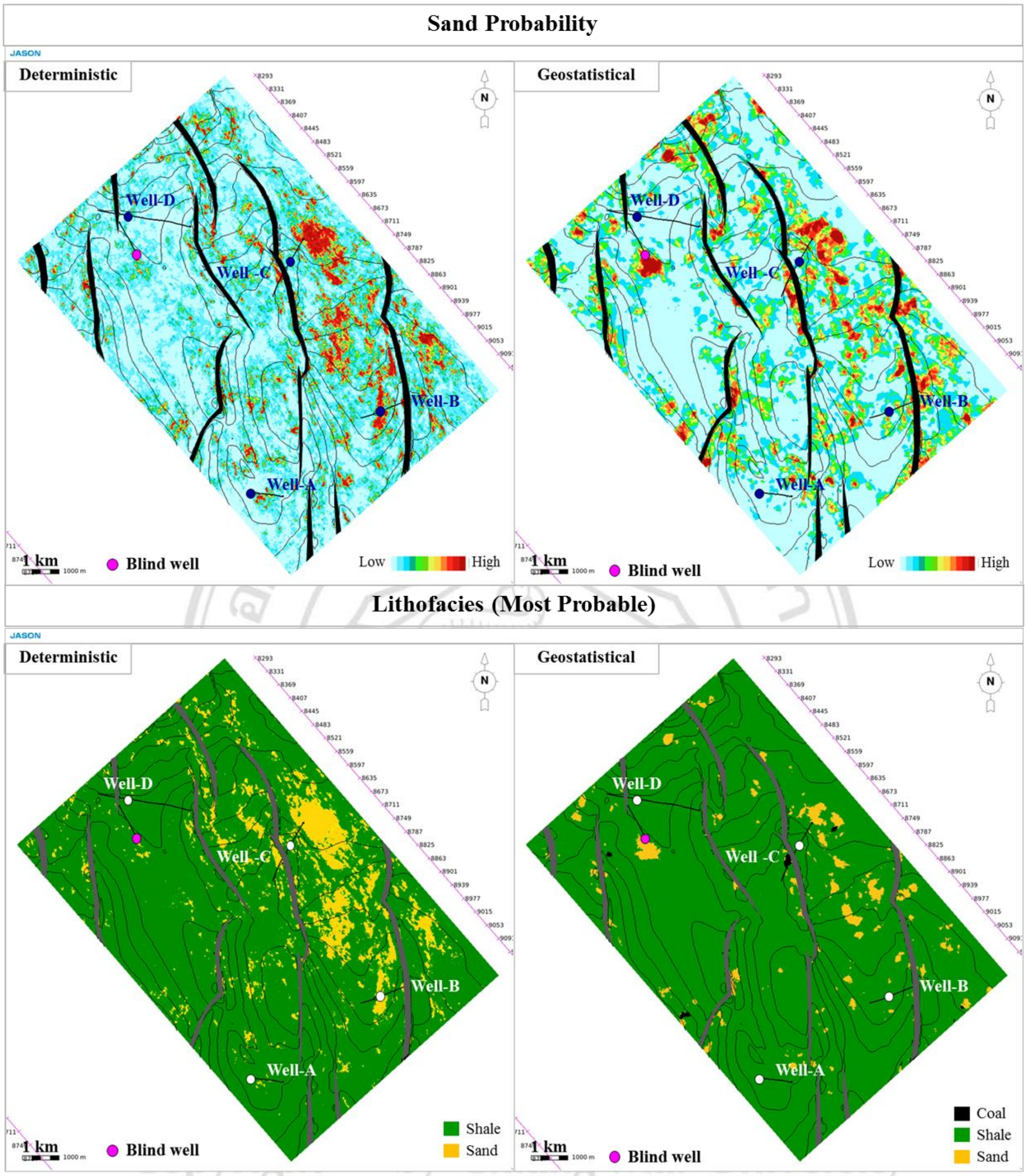

Figure 5.19 Sand probability and lithofacies slices at Reservoir 1-2 layer (H30) from deterministic (left) and geostatistical inversion (right).

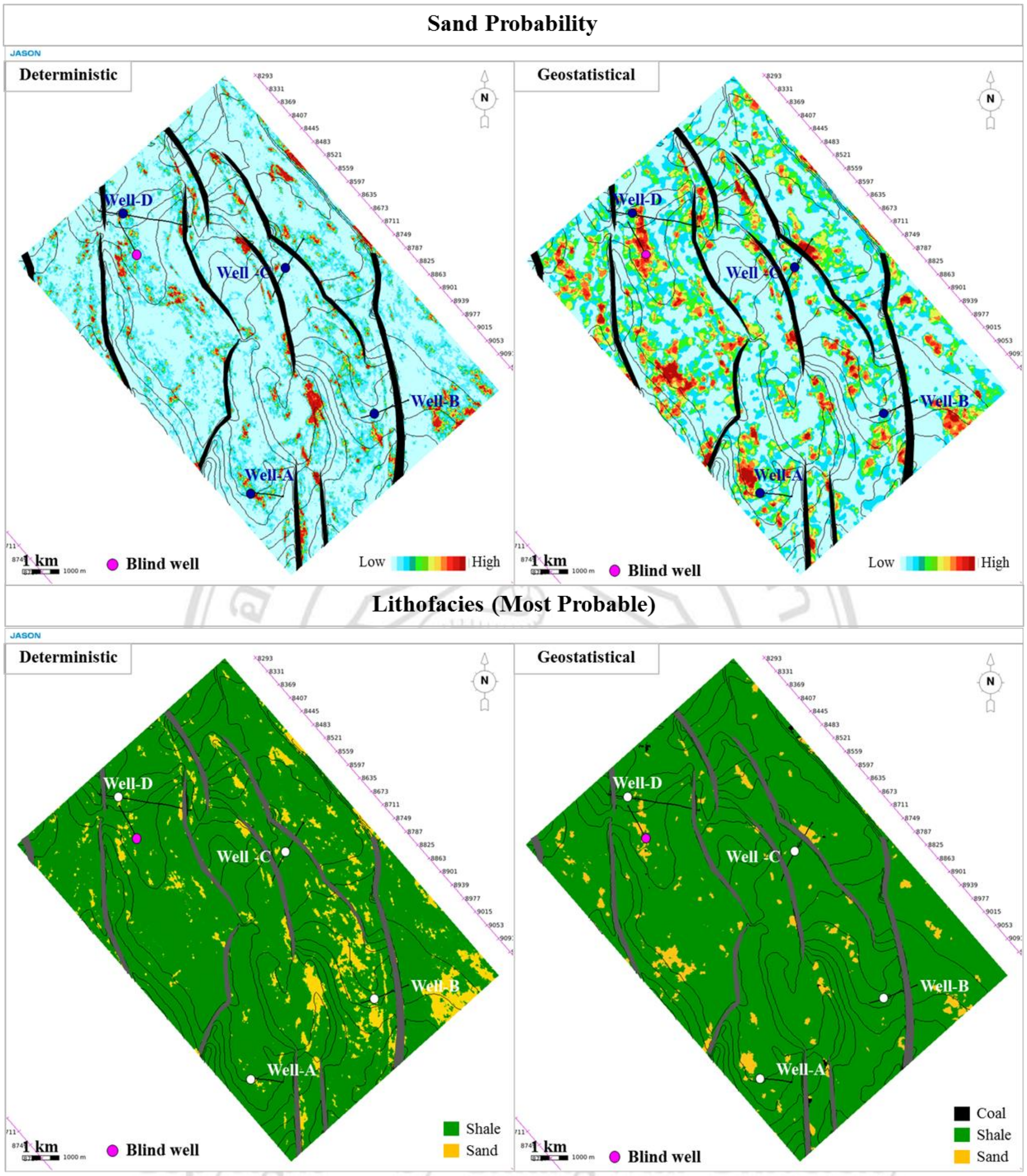

Figure 5.20 Sand probability and lithofacies slices at Reservoir 2-1 layer (H37) from deterministic (left) and geostatistical inversion (right).

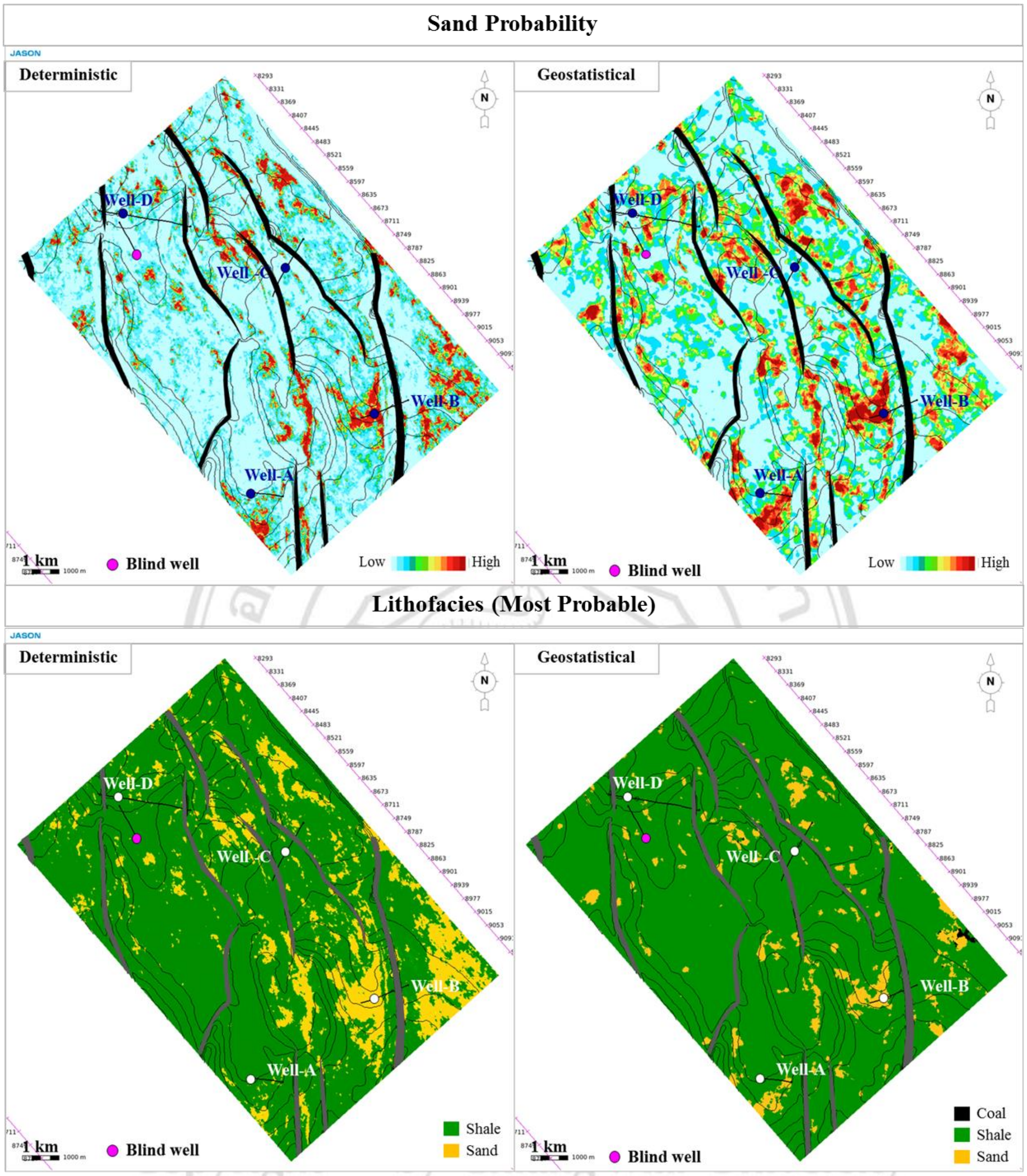

Figure 5.21 Sand probability and lithofacies slices at Reservoir 2-2 layer (H37) from deterministic (left) and geostatistical inversion (right).

5.3 Blind Well Testing

Considered as the best QC, sections of inverted properties were overlaid with blind wells to observe whether the deterministic and geostatistical inversions produced results that could be deemed satisfactory for prediction of lithology variations in the reservoirs. As demonstrated in Figure 5.22 and 5.23, blind well was overlaid on lithofacies and AI sections of deterministic and geostatistical inversion (mean case). Overall, the geostatistical provided more accurate sand prediction in term of thickness and distribution found at the blind well location. Both lithofacies and AI sections showed good correlation with the blind well, especially in the shallow reservoir section (H30), as is captured thin sand reservoirs that were beyond seismic resolution. In addition, inverted AI from both geostatistical inversion and deterministic inversion were compared as show in Figure 5.24. Inverted AI from geostatistical inversion can capture thin-bedded layers. Moreover, L1-norm (Least absolute errors) were calculated for both inverted AI from geostatistical inversion and deterministic inversion. Geostatistical inversion (L1-norm= 190,055) showed better match with measured AI log that provided lower L1-norm than deterministic inversion (L1-norm = 257,340).

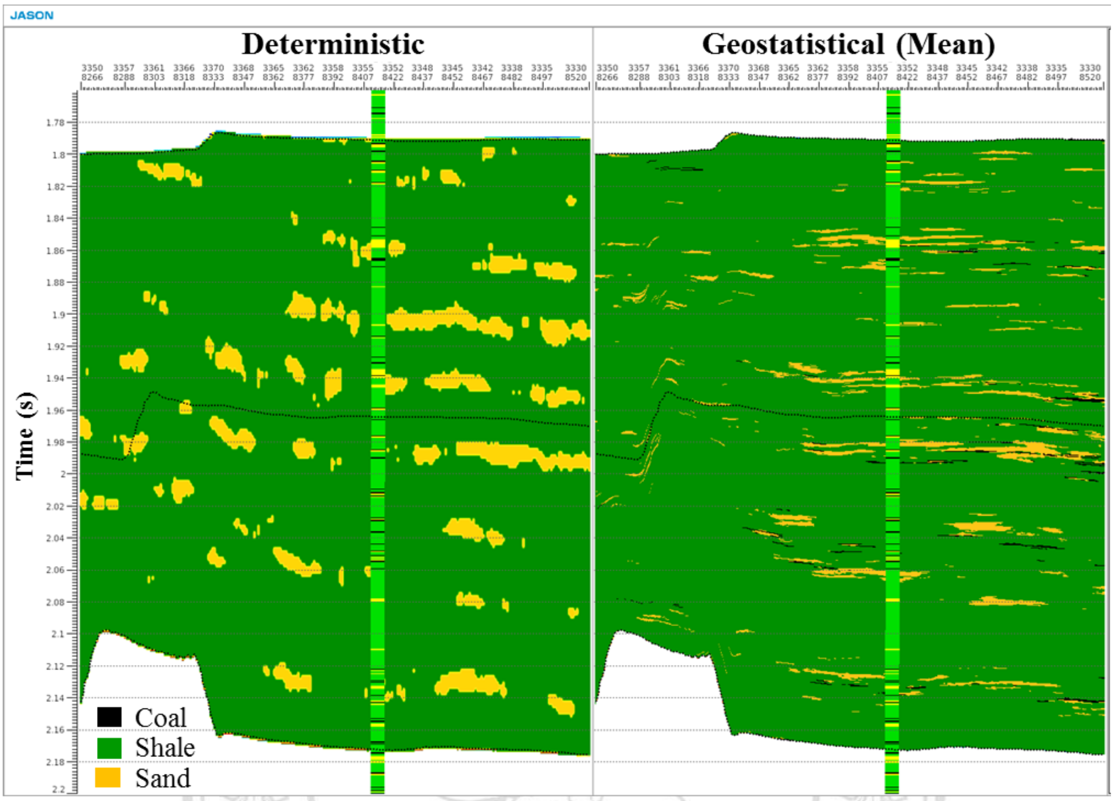

Figure 5.22 Lithofacies section overlaid with bind well.

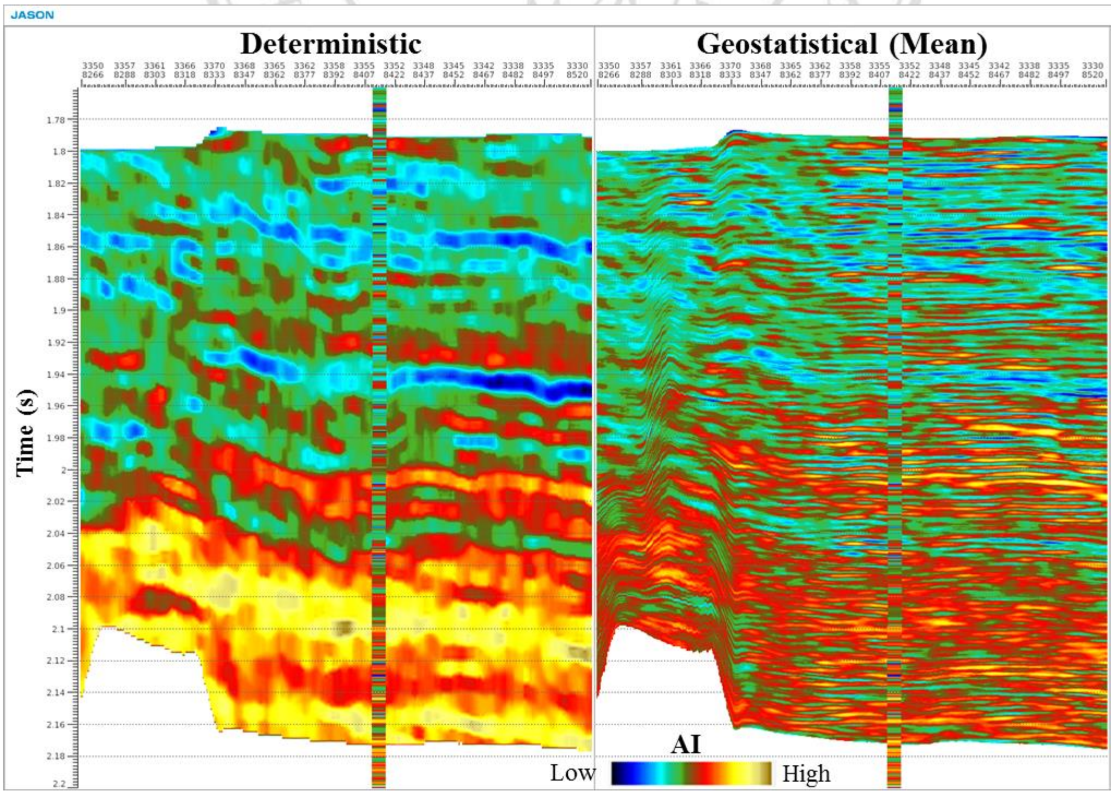

Figure 5.23 P-Impedance section overlaid with bind well.

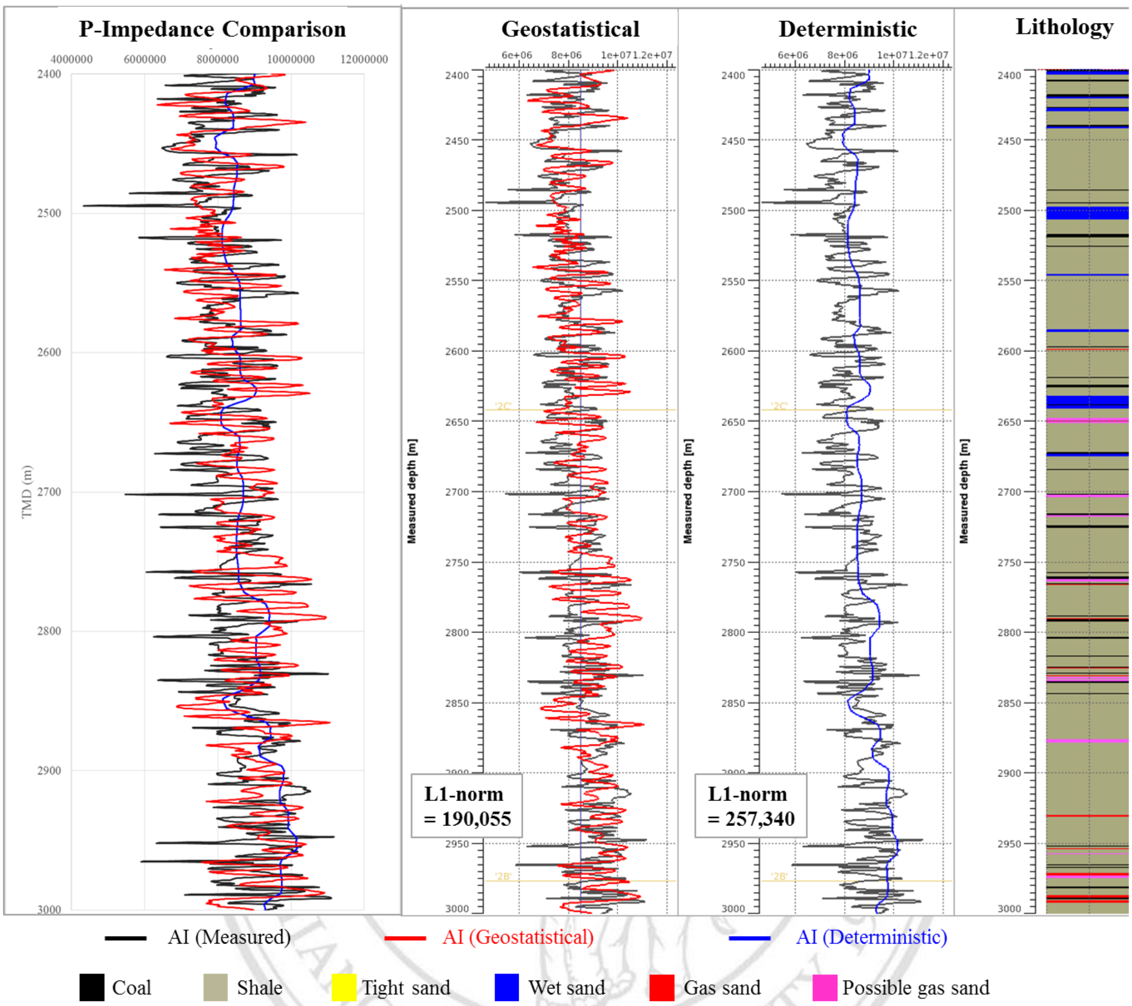

Figure 5.24 P-Impedance (AI) comparison among measured AI, inverted AI from geostatistical inversion and inverted AI from deterministic inversion.